

Effect of oxygen reduction on the optical conductivity of $\text{La}_{0.75}\text{Ca}_{0.25}\text{MnO}_3$

A. Nucara, A. Perucchi, and P. Calvani

*“Coherentia”—Istituto Nazionale di Fisica della Materia and Dipartimento di Fisica, Università di Roma “La Sapienza,”
Piazzale A. Moro 2, I-00185 Roma, Italy*

T. Aselage

Sandia National Laboratories, Albuquerque, New Mexico 87185-0613, USA

D. Emin

Department of Physics and Astronomy, University of New Mexico, Albuquerque, New Mexico 87131-1156, USA

(Received 24 February 2003; published 26 November 2003)

Reflectivity measurements are used to obtain the optical conductivity of three $\text{La}_{0.75}\text{Ca}_{0.25}\text{MnO}_{3-y}$ samples annealed under increasingly strong reducing conditions. All three samples are nearly saturated ferromagnets although their Curie temperatures fall progressively from $T_c=221$ K to $T_c=187$ K with maximum deoxygenation. The presence of Drude absorption indicates that the unreduced and the slightly reduced samples are electrical conductors below T_c . However, the most reduced sample manifests an insulatinglike optical conductivity at all temperatures. Thus, ferromagnetism and insulating behavior coexist in the most-reduced sample. This result contradicts the notion that mobile charge carriers of an electrically conducting manganite induce its ferromagnetism. Beyond Drude absorption, midinfrared and near-infrared absorptions are also observed. A midinfrared absorption band is present in all samples. The energy at its peak falls markedly with decreasing temperature. Moreover, near-infrared absorption is found in the nonconducting sample and in the high-temperature insulating phase of the conducting samples. The implications of these findings are discussed in terms of models for properties of doped manganites.

DOI: 10.1103/PhysRevB.68.174432

PACS number(s): 75.50.Cc, 78.30.-j

I. INTRODUCTION

In the literature of colossal magnetoresistance manganites, the close interplay between transport properties and magnetic ordering observed in $A_{1-x}B_x\text{MnO}_3$ ($A=\text{La,Nd}; B=\text{Sr,Ca}$) is usually explained in terms of the magnetic double exchange (DE).^{1,2} In particular, the net transfer rate for a hole between two Mn ions increases monotonically as the alignment of these Mn magnetic moments is altered from antiparallel to parallel. The transitions from semiconducting to conducting behavior and from paramagnetism to ferromagnetic ordering are thereby linked to one another in $\text{La}_{1-x}\text{Ca}_x\text{MnO}_{3-y}$, (LCMO) with $0.2 \leq x \leq 0.48$

The bare DE mechanism, however, cannot account for electronic transport measurements in these manganites. In particular, electronic transport in the semiconducting region has long been attributed to low-mobility phonon-assisted polaronic hopping.³⁻⁶ Thus, explanation of electronic transport data requires including polaronic effects.⁷ These polaron effects include relief of the Jahn-Teller distortion of the oxygen octahedron surrounding an Mn ion when the Mn site is occupied by a hole.

In one view carrier-induced ferromagnetism is invoked to produce a transition from a low-temperature ferromagnetic conductor to a high-temperature paramagnetic semiconductor. In a polaronic DE framework, itinerant large polarons of the conducting phase may turn into hopping small polarons⁸ or bipolarons⁹ above T_c . Other authors, however, envision DE mechanism playing a minor role in carrier-induced ferromagnetism. There are indications that holes in manganites preferentially occupy oxygen ions.¹⁰ Ferromagnetism is then

hypothesized to arise from direct exchange between these holes.^{10,11} Formation of bipolaron holes would be favored under this approach.¹¹ In an alternative view the conductivity transition is driven by the magnetic transition of the underlying lattice. For example, the manganites' conductivity transition is attributed to the reduction of electronic overlap between dopant-related states that accompanies their abrupt shrinking (polaron collapse) upon the loss of a ferromagnet's long-range magnetic order.¹² This mechanism has been suggested¹³ to drive the transition from a low-temperature ferromagnetic conductor to a high-temperature paramagnetic insulator that occurs in suitably doped ferromagnetic EuO. All the above interpretations of the manganites' rich phenomenology attribute a crucial role to polaronic effects. The polaronic nature of carriers manifests itself through the presence of absorption bands in the infrared spectra.¹⁴

Thus, there have been numerous measurements of the optical properties of manganites. Early measurements on polycrystalline $\text{La}_{1-x}\text{Ca}_x\text{MnO}_3$ with $x \sim 0.3$ showed, in addition to a Drude term, the presence of midinfrared bands. Authors assigned these bands either to transitions between Mn levels,¹⁵ or to polaronic absorption.¹⁶ A transfer of a localized electron from a Mn^{+3} ion to a Mn^{+4} ion should be polaronic since Mn^{+3} ions are associated with Jahn-Teller distortions and Mn^{+4} ions are not.

Further investigations on single crystals¹⁷ or thin films¹⁸ reported good agreement with the theoretical predictions of the DE model renormalized by electron-phonon interaction.⁷ However, most of these results were subsequently questioned by a study of the reflectivity of $\text{La}_{0.825}\text{Sr}_{0.175}\text{MnO}_3$,^{19,20} whose samples were single crystals cleaved under vacuum

rather than being polished. The authors find that the optical conductivity shows just a normal Drude behavior below T_c . These authors attributed the midinfrared contributions observed below T_c in previous experiments on Ca-doped manganites to spurious effects resulting from a poor sample surface. Indeed, a recent study²¹ on a single crystal of $\text{La}_{0.735}\text{Ca}_{0.265}\text{MnO}_3$ concludes that surface polishing lowers the reflectivity $R(\omega)$ and introduces into $R(\omega)$ a dip near 0.5–0.6 eV. Both effects, shown in Fig. 2 of Ref. 21, might be used as a measure of whether a polished sample is damaged. Finally, one should mention that infrared spectroscopy has been also applied to the study of charge ordering and phase separation in $\text{La}_{1-x}\text{Ca}_x\text{MnO}_3$ with $x \geq 0.5$. In these materials, charge ordering opens optical gaps in the far infrared²² and, according to a recent paper, even in the near infrared.²³

Indeed, the magnetism, charge transport, charge ordering, and phase separation in manganites depends on dopants' concentration and size as well as on preparation conditions. Many results are summarized in the x, T phase diagram²⁴ of LCMO. In particular, a ferromagnetic insulating phase is observed²⁴ in $\text{La}_{1-x}\text{Ca}_x\text{MnO}_3$ for approximately $0.10 < x < 0.20$ and $T < 160$ K. This feature indicates that a manganite's ferromagnetism can occur without mobile carriers.

Long ago Jonker²⁵ emphasized that the Curie temperature in manganites depends strongly on the size of the divalent ion (Ca, Sr, or Ba). He suggested that ferromagnetism is stabilized by dopant-induced strains rather than by the carriers the dopants introduce. If true, a conducting ferromagnetic manganite can be converted into a ferromagnetic insulator by just reducing the number of its carriers. This reduction may be accomplished by introducing oxygen vacancies since they tend to compensate the charge carriers introduced by Ca doping. In fact, deoxygenation can introduce moderate densities of oxygen vacancies without producing phase separation.

In principle, each substitution of a Ca^{2+} ion for a La^{2+} ion in $\text{La}_{1-x}\text{Ca}_x\text{MnO}_{3-y}$ will produce a hole. However, at the very high Ca concentration considered here, $x = 0.25$, holes may be trapped by clusters of Ca ions. In particular, random substitutions of Ca for La result in 82% of unit cells with a Ca ion being adjacent to at least one other cell with a Ca substitution. Thus, the number of active carriers per formula unit is presumed to be lower than x . In addition, the hole concentration is further reduced by deoxygenation since it produces oxygen vacancies that tend to trap holes, thereby compensating them.

Experiments performed on samples of $\text{La}_{1-x}\text{Ca}_x\text{MnO}_{3-y}$ with different x and y ,⁶ showed that ferromagnetism persists in the semiconducting state of LCMO. Recently, a detailed study of magnetism, dc transport, and Seebeck coefficient in the same system²⁶ confirmed that de-oxygenation can produce a single-phase semiconductor with fully saturated ferromagnetism. Previously, the effect of de-oxygenation on the magnetic and electronic transport properties of manganites was investigated in $\text{La}_{0.67}\text{Ba}_{0.33}\text{MnO}_{3-y}$ for²⁷ y ranging from 0.01 to 0.02. Deoxygenation was also attained in $\text{La}_{1-x}\text{Sr}_x\text{MnO}_{3+y}$, over a wide x range²⁸ when $y < 0$.

The infrared reflectivity of $\text{La}_{1-x}\text{Sr}_x\text{MnO}_3$ was measured as a function of x through the transition between the ferro-

TABLE I. Properties of the three $\text{La}_{0.75}\text{Ca}_{0.25}\text{MnO}_{3-y}$ samples investigated here. $P(\text{O}_2)$ is the oxygen pressure during the annealing (see text), y is the resulting oxygen defect. V is the cell volume as determined by x-ray analysis. T_c is the Curie temperature and N_B is the number of Bohr magnetons per formula unit at saturation, 5 K.

Sample	$P(\text{O}_2)$ (atm)	y	$V(\text{nm}^3)$	T_c (K)	N_B
A	1	0.011	0.23339	221	3.8
B	10^{-4}	0.011	0.23358	208	3.8
C	$10^{-7.8}$	0.04	0.23380	187	3.6

magnetic insulating phase and the metallic phase.²⁹ When the temperature was decreased below T_c a strong Drude term emerged for $x = 0.175$. By contrast, decreasing the temperature below T_c for a sample with $x = 0.10$ only increased the spectral weight of the midinfrared absorption.

Here we study how the infrared properties of a manganite behave upon the introduction of oxygen vacancies. In particular, we report on the evolution of the optical conductivity of $\text{La}_{0.75}\text{Ca}_{0.25}\text{MnO}_{3-y}$ for increasing y . To our knowledge, this is the first systematic study of infrared spectra as a function of oxygen vacancy concentration at a constant doping level. The loss of a Drude contribution confirms that deoxygenation converts a manganite from being a ferromagnetic conductor into a ferromagnetic semiconductor. Moreover, we find that a midinfrared absorption band persists in conducting and semiconducting samples although the band shifts strongly to lower energies with decreasing temperature. Finally, near-infrared absorption diminishes upon passing from the insulating phase to the conducting phase.

II. EXPERIMENT

Preparation of the $\text{La}_{0.75}\text{Ca}_{0.25}\text{MnO}_3$ samples used in our measurements is described in detail in Ref. 26. Briefly, amorphous precursors produced by aqueous coprecipitation were calcined to produce single-phase manganite powders. These powders were pressed into pellets and sintered at 1350°C for 2 h in flowing O_2 , then cooled slowly to room temperature. Oxygen vacancies were subsequently introduced and controlled by annealing samples at 1200°C in an ambient of low, fixed oxygen partial pressure $P(\text{O}_2)$.

X-ray diffraction confirmed that manganite samples with modest deoxygenation were single phase.²⁶ The structural and magnetic properties of single-phase $\text{La}_{0.75}\text{Ca}_{0.25}\text{MnO}$ samples produced under three different annealing conditions are listed in Table I. Labels A, B, and C in Table I are used to designate annealing conditions of the three samples studied herein.

The magnetizations of samples produced under the three annealing conditions, A through C, of Table I are plotted versus temperature in Fig. 1, reproduced from Ref. 26. All samples exhibit a sharp ferromagnetic transition. However, their Curie temperatures T_c (reported in Table I) decrease from A to C. The magnetic moments per formula unit N_B , in terms of Bohr magnetons, for the three samples are also reported in the table. As expected, the observed values of N_B are modestly reduced from their ideal insulating value 4 by

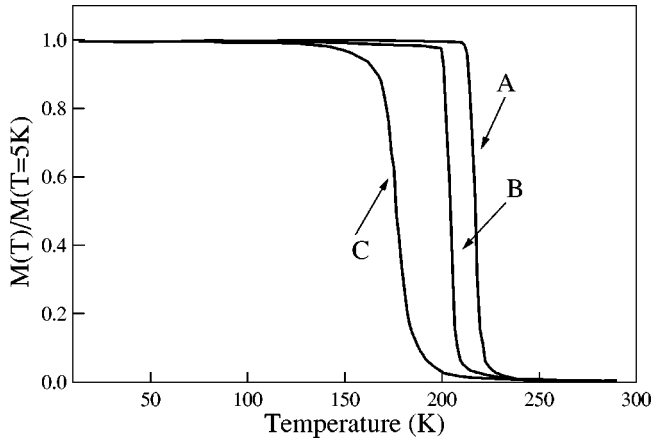


FIG. 1. Magnetic moments of the three $\text{La}_{0.75}\text{Ca}_{0.25}\text{MnO}_{3-y}$ samples with different y , normalized to the respective saturation values at 5 K. The data are obtained upon cooling the samples from room temperature in a field of 100 Oe.

hole doping and are only slightly affected by oxygen reduction. In particular, N_B for sample C, with an oxygen deficiency $y = 0.04$, is only 5% lower than that of unreduced sample A.

The reflectivity $R(\omega)$ of each pellet was measured at nearly normal incidence from a carefully polished surface. The reference mirror was obtained by evaporating a gold film onto the sample itself,³⁰ in order to avoid errors due to residual irregularities of the surface. Data were collected by a rapid-scanning interferometer between 130 and $10\,500\text{ cm}^{-1}$ and by thermoregulating the samples within $\pm 2\text{ K}$ between 290 and 45 K.

The polycrystalline nature of the material may be a source of errors when extracting the optical conductivity $\sigma(\omega)$ from $R(\omega)$ by Kramers-Kronig transformations if the transport properties are strongly anisotropic.³¹ In the present case, the pseudocubic, nearly isotropic, structure of the La-Ca manganite should preclude the occurrence of such errors. In any case, here $\sigma(\omega)$ was extracted from $R(\omega)$ by fitting the data to a Drude-Lorentz model. This procedure makes strong assumptions on the asymptotic behavior of $R(\omega)$ unnecessary. The model dielectric function was

$$\tilde{\epsilon}(\omega) = \epsilon_\infty - \frac{\omega_p^2}{\omega^2 - i\omega\Gamma_D} + \sum_{j=1}^{n_{ph}} \frac{S_j^2}{(\omega_j^2 - \omega^2) - i\omega\Gamma_j} + \sum_{k=1}^{n_{hfo}} \frac{S_k^2}{(\omega_k^2 - \omega^2) - i\omega\Gamma_k}. \quad (1)$$

Here, the first contribution on the right represents contributions from frequencies above the measuring range. The second term is the carriers' Drude contribution with plasma frequency ω_p and relaxation rate Γ_D . The third term depicts the net contribution from phonons, designated by the index j , with strength S_j and width Γ_j . The final term sums the contributions of the high-frequency oscillators (hfo) detected in the midinfrared and the near-infrared. We always chose the

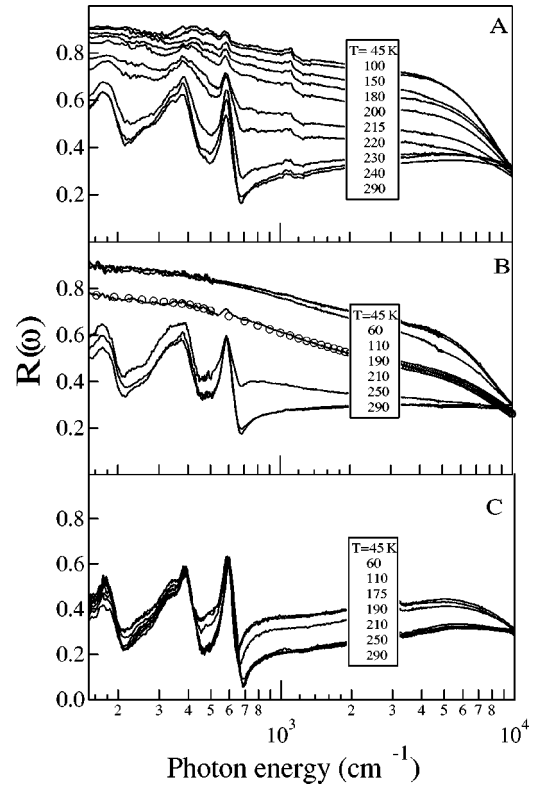


FIG. 2. Reflectivity $R(\omega)$ of the three $\text{La}_{0.75}\text{Ca}_{0.25}\text{MnO}_{3-y}$ samples with oxygen deficiency y increasing from top to bottom. An example of fitting curve, with a reduced density of points for the reader's convenience, is shown for sample B at 190 K.

fit which allowed us to satisfactorily reproduce the data by using the minimum number of oscillators.

Equation (1) is used to model the complex refraction index \tilde{n} which is then introduced into the expression for the reflectivity at normal incidence (8° in our case)

$$R(\omega) = \frac{[\tilde{n}(\omega) - 1]^2}{[\tilde{n}(\omega) + 1]^2}. \quad (2)$$

III. RESULTS

The reflectivities $R(\omega)$ of the three $\text{La}_{0.75}\text{Ca}_{0.25}\text{MnO}_{3-y}$ samples are plotted against the logarithm of the frequency in Fig. 2 for temperatures from 45 to 290 K. The low-temperature reflectivities of samples A and B are slightly higher at all infrared frequencies than that reported in Ref. 17 for a high-quality single crystal of $\text{La}_{0.67}\text{Ca}_{0.33}\text{MnO}_3$. These reflectivities are also quite similar to that reported in Ref. 21 for a good single crystal of $\text{La}_{0.735}\text{Ca}_{0.265}\text{MnO}_3$ that was annealed after polishing. We cannot anneal polished films in oxygen since the purpose of our study is to determine how carefully controlled de-oxygenation of a manganite affects its optical properties. However, not only $R(\omega)$ is high, but no dip in the midinfrared is observed in Fig. 2 like that reported in Ref. 21 to indicate surface damage.²¹ These observations indicate the good optical quality of the present samples and the reliability of data reported in Fig. 2.

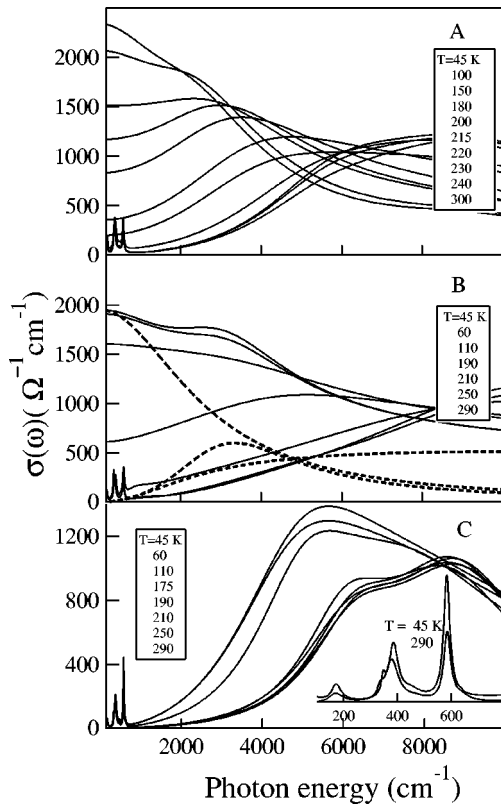


FIG. 3. Optical conductivity $\sigma(\omega)$ extracted from the $R(\omega)$ of Fig. 2 for the $\text{La}_{0.75}\text{Ca}_{0.25}\text{MnO}_{3-y}$ samples with y increasing from top to bottom. An example of decomposition of $\sigma(\omega)$ into a Drude plus two Lorentzian contributions is shown for sample *B* at 45 K. The inset of the bottom panel shows the far-infrared spectrum of sample *C*, at two temperatures, on an expanded scale.

The raw data in Fig. 2 show that, for samples *A* and *B*, $R(\omega)$ becomes increasingly conductinglike, as T is lowered below T_c . Correspondingly, one observes a strong screening of these samples' phonon absorption lines at low temperatures. However, above T_c , $R(\omega)$ is insulatinglike in both samples, with well-defined phonon lines. By contrast, the reflectivity of the most-reduced sample, sample *C*, is insulatinglike at all temperatures, and does not manifest screening of the phonon absorption lines. In *C*, moreover, a broad mid-infrared contribution springs up at low temperature.

The optical conductivity $\sigma(\omega)$ was extracted at all temperatures from $R(\omega)$ by fits as good as that shown for sample *B* at 190 K in Fig. 2. The results are reported in Fig. 3, which depicts the above findings in greater detail. At room temperature in the paramagnetic phase all samples show three well-defined phonon peaks, shown for sample *C* on an expanded scale in the inset of the bottom panel. In all samples, two TO modes appear at 170 and 577 cm^{-1} in agreement with previous observations at $x=0.3$ (Ref. 32) and $x=0.33$.¹⁷ On the other hand, the fine structure of the central peak with modes at 340 and 370 cm^{-1} was previously resolved only in a single crystal with $x=0.33$.¹⁷ A fifth (weak) phonon contribution is detected at $\sim 270 \text{ cm}^{-1}$, so $n_{ph}=5$ in Eq. (1). In the midinfrared, the spectra of all samples show a strong absorption that can be fit by two

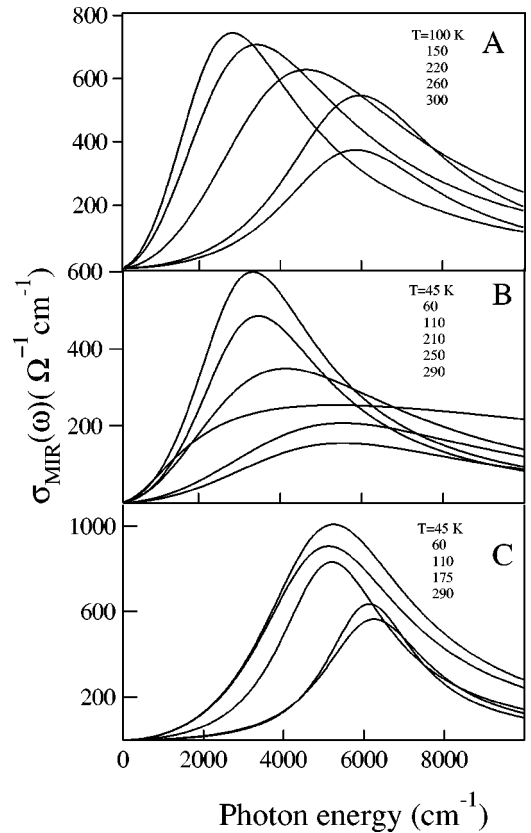


FIG. 4. The midinfrared contribution $\sigma_{MIR}(\omega)$, as obtained from a Drude-Lorentz fit to $\sigma(\omega)$, is reported as a function of temperature for the $\text{La}_{0.75}\text{Ca}_{0.25}\text{MnO}_{3-y}$ samples with y increasing from top to bottom.

broad Lorentzian peaks. In Fig. 3, those two contributions, centered at ~ 6000 and 9500 cm^{-1} , are separated in the high-temperature paramagnetic phase of sample *C*. In samples *A* and *B* the use of two midinfrared oscillators is required by the fit, while the Drude term can be distinguished from the midinfrared absorption at the lowest temperatures. An example of decomposition of $\sigma(\omega)$ into a Drude and two Lorentzian contributions, according to Eq. (1), is shown for sample *B* at 45 K.

As T decreases below T_c , the optical conductivities of samples *A* and *B* behave similarly. A strong Drude contribution grows with decreasing temperature. In addition, the midinfrared bands in both samples progressively shift to lower energy as the temperature is decreased. The shifts of these midinfrared absorption bands to lower energy with decreasing temperatures are evident in the curves of Fig. 4, where just the midinfrared bands obtained from the Drude-Lorentz fit to our data are shown for different temperatures. The mid-infrared peaks of samples *A* and *B* fall to $\sim 2500\text{--}3000 \text{ cm}^{-1}$ at the lowest temperature (45 K).

The conductivity of sample *C* (bottom panel of Fig. 3) also changes with temperature. In particular, as the temperature is reduced through the Curie temperature (187 K) the bands at 6000 and 9500 cm^{-1} merge into a single peak. The energy of this peak then decreases moderately as the temperature is lowered further. On the other hand, the far-

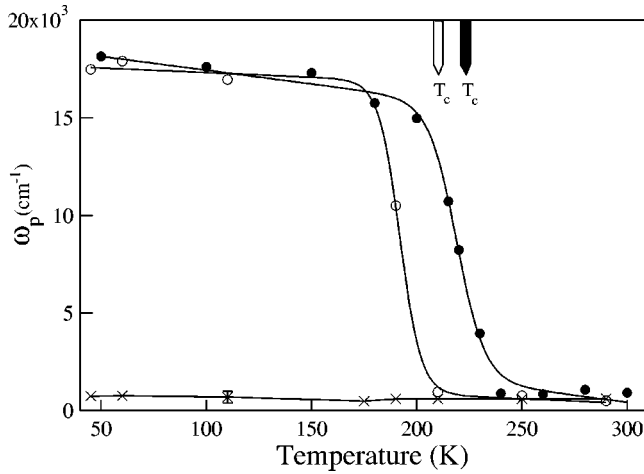


FIG. 5. Plasma frequency (ω_p) vs temperature for samples A (dots), B (circles), and C (crosses). T_c is reported for A and B by full and open arrows, respectively. The fit indicates a very small plasma frequency, with an indetermination reported by the error bar, also for sample C, even if its dc resistivity is very high at all temperatures. The lines are guides to the eye.

infrared portion of the spectrum exhibits no temperature dependence. In particular, no appreciable Drude contribution arises as the temperature is lowered below T_c , as previously observed in Ref. 29 for the ferromagnetic insulator $\text{La}_{0.9}\text{Sr}_{0.1}\text{MnO}_3$. In other words, the optical conductivity of sample C is insulatinglike down to the lowest temperature measured (45 K).

The conducting behaviors of samples A and B below T_c can be characterized with the parameters that define their Drude contribution to Eq. (1). In both samples, the Drude linewidth $\Gamma_D \sim 2000 \text{ cm}^{-1}$ below 150 K. This large value can be partially explained by the polycrystalline nature of the material. More meaningful for the present study is the behavior of the plasma frequency ω_p , which is plotted versus temperature for both A and B in Fig. 5. For comparison, their Curie temperatures (from Table I) are indicated with arrows. The plasma frequency of sample A increases rapidly in the vicinity of the Curie temperature T_c . However, the rapid rise of the plasma frequency of sample B occurs somewhat below T_c . Even the largest plasma frequencies of these doped magnetic insulators are below those of many conventional metals. However, the plasma frequencies measured in the low-temperature conducting regime are much higher than can be attributed to the collective motion of self-trapped carriers, where ω_p is comparable to a characteristic vibrational frequency.³³ Whether their motion is individual or collective, self-trapped carriers cannot move any faster than the atoms whose displacements are responsible for the self-trapping of carriers.

The Drude-Lorentz fit to $\sigma(\omega)$ generates the midinfrared (MIR) absorption bands depicted in Fig. 4. At room temperature, the highest temperature measured, the MIR absorption is centered at $\sim 6000 \text{ cm}^{-1}$. It is evident that the MIR absorption bands depicted in Fig. 4 shift with temperature. One means to quantify these shifts is to first calculate the first moment of the MIR absorption,

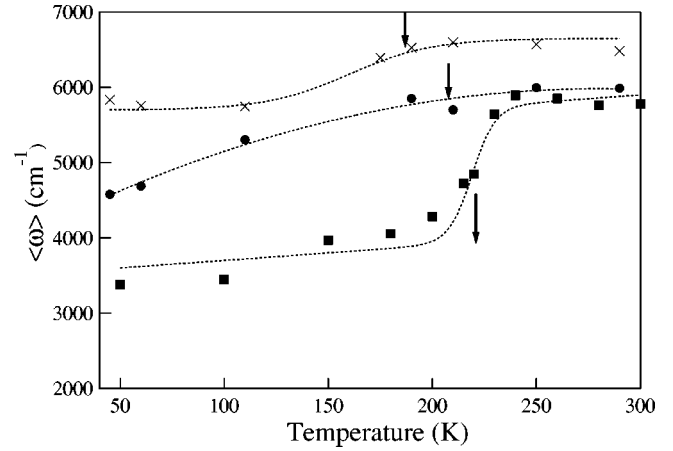


FIG. 6. First moment of the midinfrared band of Fig. 4 vs temperature, for the samples A (squares), B (circles), and C (crosses). The arrows mark T_c for all samples. The lines are guides to the eye.

$$\langle \omega \rangle = \frac{\int_0^{\omega^*} \omega \sigma_{MIR}(\omega) d\omega}{\int_0^{\omega^*} \sigma_{MIR}(\omega) d\omega}, \quad (3)$$

where $\omega^* = 10500 \text{ cm}^{-1}$ is the maximum frequency measured in our experiments. The temperature dependence of each sample's first moment is then displayed in Fig. 6. The first moments of all samples fall with decreasing temperature. Sample A manifests the most pronounced overall decline of a sample's first moment. Its fall is most rapid in the vicinity of the Curie temperature. Sample A is fully oxygenated and has the highest low-temperature bulk electrical conductivity.²⁶

Finally, the third major contribution to the Drude-Lorentz fit of the optical conductivity comes from a near-infrared (NIR) absorption band centered at a doping-dependent $\omega_{NIR} > 8000 \text{ cm}^{-1}$. However, a NIR band is only resolved in the conductivity of sample C, Fig. 3.

We now address how the relative contributions of the Drude, MIR, and NIR bands to the conductivity change with temperature. To begin, we define the effective number of carriers

$$n_{eff} = \frac{2m^*V}{\pi e^2} \int_0^{\omega^*} \sigma(\omega) d\omega, \quad (4)$$

where e and m^* are an electron's charge and effective mass and V is the volume of a unit cell. The integration limit ω^* is the maximum frequency of our measurements, 10500 cm^{-1} . Since $\sigma(\omega)$ is the sum of $\sigma_{Drude}(\omega)$, $\sigma_{MIR}(\omega)$, and $\sigma_{NIR}(\omega)$, separate integrations of each of these components yields the contributions of the Drude, MIR, and NIR bands to n_{eff} . The fractional contribution of each of these bands to n_{eff} is shown as a function of temperature in Fig. 7 for samples A and B. We see that the transfer of spectral weight between the Drude and NIR absorptions primarily occurs in the vicinity of the Curie temperature. By contrast, the spec-

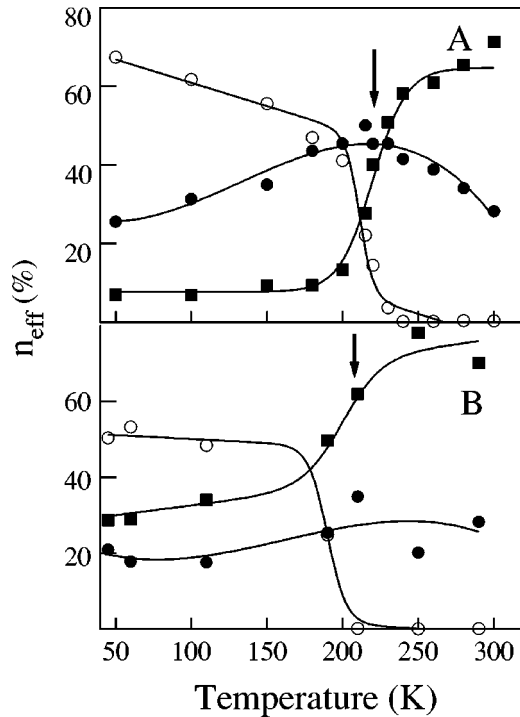


FIG. 7. Relative contribution vs temperature of the Drude (open circles), MIR (full circles), and NIR bands (squares) to the effective number of carriers n_{eff} for samples A (top) and B (bottom). The arrows mark T_c for both samples. The lines are guides to the eye.

tral weight of the MIR band changes relatively little with temperature and is not even strongly affected by magnetic ordering.

IV. SUMMARY AND CONCLUSIONS

We now summarize our principal observations. The implications of our findings for models of the properties of doped manganites are also discussed.

Doped lanthanum manganites are ferromagnets that usually are electrically conducting below their Curie temperature and semiconducting above their Curie temperature. However, they also exhibit ferromagnetic insulating phases when the divalent ion concentration is reduced to about 0.10–0.15. Here we have discussed how the magnetic and the optical properties of a LCMO change when it is deoxygenated at constant Ca doping, $x=0.25$. This procedure is expected to alter the carrier concentration while not affecting the dopant-related strains that have been hypothesized as stabilizing manganites' ferromagnetism.²⁵

We find that $\text{La}_{1-x}\text{Ca}_x\text{MnO}_{3-y}$ remains a single-phase fully saturated ferromagnet, albeit with slightly lowered Curie temperature, after modest deoxygenation. However, our reflectivity measurements show that the low-temperature, $T < T_c$, conducting behavior is lost after this modest deoxygenation. In particular, this de-oxygenation eliminates any indication of an appreciable Drude absorption. This observation complements dc electrical transport measurements that show low-temperature, $T < T_c$, semiconducting behavior (rather than conducting behavior) for these deoxygenated

materials.²⁶ Thus, optical and dc transport measurements both show $x \sim 0.25$ LCMO being ferromagnetic even when it is semiconducting. We conclude that double exchange with itinerant charge carriers of the conducting phase is not the cause of these manganites' ferromagnetism.

The parameters we obtain for the Drude absorption of the conducting phases of samples A and B are also significant. In particular, our analysis yields both a large plasma frequency and a large scattering rate for the Drude absorption. The plasma frequency, about $20\,000\text{ cm}^{-1}$ at low temperatures, while below that of many metals, is consistent with a moderate density of freely moving carriers. By contrast, were the carriers "self-trapped" their "plasma frequency" would not exceed a characteristic vibrational frequency since self-trapped carriers are constrained to follow atomic motions.³³ Furthermore, the very large low-frequency effective mass of coherently moving self-trapped carriers results in their being only weakly scattered (with a scattering rate below the characteristic vibration frequency).³³ We conclude that the carriers that produce the Drude absorption we observe are not self-trapped. Rather, these charge carriers can only be "weakly coupled" to atomic vibrations. Thus, absorption bands that indicate strong coupling to atoms' vibrations do not emanate from our mobile charge carriers.

We observe midinfrared and near-infrared absorption in all samples. In the two samples with a conductivity transition near T_c , the spectral weight of the near-infrared absorption falls dramatically as the temperature passes below the Curie temperature. In the sample that remains semiconducting even below T_c , the near-infrared absorption appears temperature independent. These results suggest that absorption in the near infrared is associated with semiconducting manganites. Prior work hypothesized that this near-infrared absorption band originates from on-site transitions between e_g^1 and e_g^2 levels at Mn^{+3} sites.¹⁵ Although these transitions are forbidden on the isolated ion, Mn-O hybridization is presumed to permit them in manganites.

The conductivity transition near T_c has little effect on the spectral weight of the midinfrared absorption. By itself, this result suggests that the midinfrared absorption is not associated with charge transfer between magnetic ions since a change of magnetic ordering necessarily affects the probability of such charge transfer. Nonetheless, the midinfrared absorption has previously been attributed to charge transfer between Mn^{3+} and Mn^{4+} sites.¹⁵ Our results also challenge this assignment.

Finally, we observe the midinfrared absorption band shifting to lower energies (by $1000\text{--}4000\text{ cm}^{-1}$) as the temperature is lowered below T_c . Such shifts occur even in the absence of a low-temperature conducting phase. Thus, these midinfrared shifts seem related to magnetic order. The corresponding energy gap between the initial and final electronic states therefore increases with the onset of magnetic disorder. This result is consistent with a succession of polaronic collapses in which the imposition of magnetic disorder progressively triggers electrons' states to abruptly fall in energy as they become more localized.^{12,13} All told, the present study addresses how the optical properties of a ferromagnetic Ca-doped manganite are affected by oxygen re-

duction. We find that the double exchange mechanism does not play an important role in producing ferromagnetism in these manganites. The present measurements and their analysis also enable us to characterize how the Drude, far-infrared, and midinfrared contributions each depend on magnetic

order and on carrier density. Taken together these dependencies help identify the processes that produce these optical responses. While these identifications are helpful, much work is still needed in order to understand these complex materials.

- ¹C. Zener, Phys. Rev. **82**, 403 (1951).
- ²P.W. Anderson and H. Hasegawa, Phys. Rev. **100**, 675 (1955).
- ³J. Volger, Physica (Amsterdam) **20**, 49 (1954).
- ⁴R.C. Miller, R.R. Heikes, and R. Mazelsky, J. Appl. Phys. **32**, 2202 (1961).
- ⁵M. Kertesz, I. Riess, D.S. Tannhauser, R. Langpape, and F.J. Rohr, J. Solid State Chem. **42**, 125 (1982).
- ⁶J. Tanaka, M. Umehara, S. Tamura, M. Tsukioka, and S. Ehara, J. Phys. Soc. Jpn. **51**, 1236 (1982).
- ⁷A.J. Millis, B.I. Shraiman, and R. Mueller, Phys. Rev. Lett. **77**, 175 (1996).
- ⁸C.A. Perroni, G. De Filippis, V. Cataudella, and G. Iadonisi, Phys. Rev. B **64**, 144302 (2001).
- ⁹G. Zhao, D.J. Kang, W. Prellier, M. Rajeswari, H. Keller, T. Venkatesan, and R.L. Greene, Phys. Rev. B **63**, 060402(R) (2000).
- ¹⁰H.L. Ju, H.-C. Sohn, and K.M. Krishnan, Phys. Rev. Lett. **79**, 3230 (1997).
- ¹¹A.S. Alexandrov and A.M. Bratkovsky, Phys. Rev. Lett. **82**, 141 (1999).
- ¹²D. Emin, in *Science and Technology of Magnetic Oxides*, edited by M.F. Hundley, J.H. Nickel, R. Ramesh, and Y. Tokura, Mater. Res. Soc. Symp. Proc. **494** (Materials Research Society, Pittsburgh, 1998), pp. 163–174.
- ¹³D. Emin, M.S. Hillery, and N.L.H. Liu, Phys. Rev. B **33**, 2933 (1986); M.S. Hillery, D. Emin, and N.H. Liu, Phys. Rev. B **38**, 9771 (1988).
- ¹⁴P. Calvani, Riv. Nuovo Cimento **8**, 1 (2001).
- ¹⁵J.H. Jung, K.H. Kim, T.W. Noh, E.J. Choi, and J. Yu, Phys. Rev. B **57**, R11 043 (1998).
- ¹⁶K.H. Kim, J.H. Jung, and T.W. Noh, Phys. Rev. Lett. **81**, 1517 (1998).
- ¹⁷A.V. Boris, N.N. Kovaleva, A.W. Bazhenov, P.J.M. Van Bentum, Th. Rasing, S.-W. Cheong, A.V. Samoilov, and N.-C. Yeh, Phys. Rev. B **59**, R697 (1999).
- ¹⁸M. Quijada, J. Cerne, J.R. Simpson, H.D. Drew, K.H. Ahn, A.J. Millis, R. Shreekala, R. Ramesh, M. Rajeswari, and T. Venkatesan, Phys. Rev. B **58**, 16 093 (1998).
- ¹⁹K. Takenaka, Y. Sawaki, and S. Sugai, Phys. Rev. B **60**, 13 011 (1999).
- ²⁰K. Takenaka, Y. Sawaki, R. Shiozaki, and S. Sugai, Phys. Rev. B **62**, 13 864 (2000).
- ²¹O. Ripeka Mercier, R.G. Buckley, A. Bittar, H.J. Trodahl, E.M. Haines, J.B. Metson, and Y. Tomioka, Phys. Rev. B **64**, 035106 (2001).
- ²²P. Calvani, G. De Marzi, P. Dore, S. Lupi, P. Maselli, F. D'Amore, S. Gagliardi, and S.-W. Cheong, Phys. Rev. Lett. **81**, 4504 (1998).
- ²³K.H. Kim, S. Lee, T.W. Noh, and S.-W. Cheong, Phys. Rev. Lett. **88**, 167204 (2002).
- ²⁴P. Schiffer, A.P. Ramirez, W. Bao, and S.-W. Cheong, Phys. Rev. Lett. **75**, 3336 (1995).
- ²⁵G.H. Jonker, Physica (Amsterdam) **22**, 707 (1956).
- ²⁶T.L. Aselage, D. Emin, S.S. McCready, E.L. Venturini, M.A. Rodriguez, J.A. Voigt, and T.J. Headley, Phys. Rev. B **68**, 134448 (2003).
- ²⁷H.L. Ju, J. Gopalakrishnan, J.L. Peng, Qi Li, G.C. Xiong, T. Venkatesan, and R.L. Greene, Phys. Rev. B **51**, 6143 (1995).
- ²⁸R. Shiozaki, K. Takenaka, Y. Sawaki, and S. Sugai, Phys. Rev. B **63**, 184419 (2001).
- ²⁹Y. Okimoto, T. Katsufuji, T. Ishikawa, T. Arima, and Y. Tokura, Phys. Rev. B **55**, 4206 (1997).
- ³⁰C.C. Homes, M. Reedik, D.A. Cradles, and T. Timusk, Appl. Opt. **32**, 2976 (1993).
- ³¹J. Orenstein and D.H. Rapkine, Phys. Rev. Lett. **60**, 968 (1988).
- ³²K.H. Kim, J.Y. Gu, H.S. Choi, G.W. Park, and T.W. Noh, Phys. Rev. Lett. **77**, 1877 (1996).
- ³³D. Emin, Phys. Rev. B **45**, 5525 (1992).